33rd Annual International Conference of the IEEE EMBS
Boston, Massachusetts USA, August 30 - September 3, 2011

Development of a Dynamic Model for Bevel-tip Flexible Needle Insertion into Soft Tissues

Amir Haddadi and Keyvan Hashtrudi-Zaad†

Abstract— **In this paper, we develop a mechanics-based dynamic model for bevel-tip flexible needle insertion into soft tissues. We use *Newton-Euler* formulation to account for the effect of actuation, friction, tissue interactions, and bevel-tip forces on the needle. The soft tissue deformation is modeled by finite element analysis, whereas the mechanics-based model is used to predict needle deflections due to bevel-tip asymmetry. The proposed needle-tissue model is then experimentally evaluated by comparing the needle deflections for various insertion depths in a tissue phantom with those achieved from simulations.**

I. INTRODUCTION

Needle insertion into soft tissue is a common procedure employed in many clinical applications such as tissue biopsy [1], brachytherapy [2], and anesthetic delivery [3]. For effective medical diagnosis and treatment, accurate targeting is of foremost importance. However, target accuracy is affected by needle deflection and tissue deformations that happen during needle insertion. Needle deflection is mainly observed in long slender needles due to bevel-tip asymmetry, and tissue deformations take place in soft tissues.

Different models have been proposed for bevel-tip flexible needle deflections which predict needle-tip deviations from the target for compensation. Webster *et al.* proposed a kinematic model for needle deflections by generalizing the standard nonholonomic unicycle and bicycle models [4]. The effect of mechanical and geometric properties of both the needle and the tissue as well as their interaction are implicitly embedded in the model parameters which need to be identified for each pair of tissue and needle [5]. In addition, this type of model is applicable when the tissue is stiff retaliative to the needle which is not valid for many biomedical applications, such as in brachytherapy where the needles are much more rigid [6]. Kataoka *et al.* proposed a model for static relationship between bevel-tip needle deflections, its thickness, and the insertion depth [7]. They assume that the transverse forces at the needle base are proportional to the insertion depth and thus, the effect of tissue is hidden in the model.

Abolhassani *et al.* proposed a static model to estimate the amount of needle deflections during needle insertion into soft tissues as a function of needle geometry and base and load forces applied to the needle, considering the needle as a cantilever beam [8]. In their model, the effect of tissue is applied through the load forces of the tissue modeled by simple parallel springs. Hauser *et al.* used a 3D kinematic model for a flexible bevel-tip needle based on circular movements of the needle with a constant curvature [9]. In this model, the effect of homogeneous material on a specified needle is applied through a curvature factor, which is assumed to be known for a set of needle and tissue under experiment.

There are important shortcomings related to the nature of the models used or the assumptions made in the above methods. For instance, the complexity of the tissue deformation and cutting forces are not modeled directly and the needle-tissue interaction is not determined by fundamentals of mechanics. Thus, the empirical parameters of these models must be estimated for a combination of specific type of needle inserted into specific material [5]. For practical implementations, a mechanics-based model is rather necessary which directly takes into account the mechanical properties of needle and tissue, separately. In addition, most of the available models describe needle deflections in static relations which do not account for the element of time. However, needle deflection and tissue deformation are dynamic processes progressing over time as a result of applied inputs and the interaction forces. Therefore, study of mechanics-based dynamic models for the coupled needle-tissue interactions are important for the analysis of system behavior over time leading to the design of suitable dynamic controllers. Unfortunately, due to inherent complexity of these models, studies on dynamic models and dynamic control of needle insertion are very limited [3].

Reed *et al.* showed that torsional friction would result in a dynamic lag between the needle-tip and the needle base angles, while the available steering methods assume a static relation [6]. Therefore, they proposed a dynamic model to describe the observed relation between the applied *torque* and the orientation of the bevel-tip. They used a simple Kelvin-Voigt model for the tissue, viscous friction for needle-tissue integrations, and neglected tissue deformations. The orientation of the bevel-tip is then controlled through the control torque applied about the needle base [6]. To the best of our knowledge, this is the only available dynamic feedback control approach to needle insertion for a mechanics-based model. More studies are required to develop dynamic models that would apply to more generic types of needles and would provide a more accurate representation of tissue behavior and yet could be used for the design of dynamic feedback controllers.

Haddadi *et al.* [10] proposed a mechanics-based dynamic model for a symmetric flexible needle by incorporating the angular-spring method [11] for the needle and a finite element model (FEM) for the soft tissue. They analyzed the

† Department of Electrical and Computer Engineering, Queen's University, Kingston, ON K7L 3N6, Canada. email: amir.haddadi@queensu.ca.

controllability of symmetric needles inserted into deformable tissues. In this paper, the model in [10] is extended to bevel-tip needles by applying the bevel-tip asymmetric force model proposed by Misra *et al.* [5], [12]. The accuracy of the model is evaluated by comparing the data collected from simulations and experiments with a flexible needle inserted into an artificial tissue phantom, made of PVC.

II. Dynamic Model of Flexible Needles in Soft Tissues

In this paper, we will analytically derive a mechanics-based dynamic model for a bevel-tip flexible needle inserted inside a soft tissue in a two-dimensional plane (2D), as illustrated in Figures 1(a)-(c). The insertion model is separated into three main sub-models, i) dynamics of the needle, ii) finite element model (FEM) of the tissue, and iii) model for bevel-tip forces. Here, we will derive the dynamics of the needle connected to a simple robot and determine needle penetrations and deflections as functions of input and interaction forces.

A. Dynamic model of flexible needles

Here we assume that the needle is connected to a robot that can apply output force and torque along and about the needle base. We will derive the dynamics of the needle by determining the needle penetration and deflection as functions the robot force and torque and the interaction forces. In order to model the dynamics of flexible needles in the plane, we take the same approach as in [11] for angular springs model of flexible needles by considering two pseudo joints along the needle and the mass of each link at its distal end as described in [10].

The unactuated pseudo joints are modeled by torsional springs which allow the needle model to conform to the bending shape of a flexible needle. Here we consider k_{b1} and k_{b2} as the stiffness of the pseudo joints and γ_1 and γ_2 as the joint angles as shown in Figure 1(a). For a rigid needle, springs are infinitely stiff, resulting in zero joint angles. A more accurate model of the needle can be obtained at the cost of higher dynamic complexity by increasing the number of pseudo joints along the needle.

In addition to the bevel-tip considerations, which will be discussed in Section IV, the proposed model has two main changes with respect to the previous model in [10] for increased consistency with practical applications. First, we use Newton-Euler formulations to model the flexible needle as a three-link manipulator with angular springs at each joint. This method can *directly* apply the effect of asymmetric needle-tip forces as well as the integrated tissue forces to obtain needle deflection as opposed to the Lagrange formulation used in [10] that could indirectly account for these effects. Second, we included a revolute-prismatic (RP) planar robot holding the needle at its base as shown in Figure 1(a). The needle is also considered as a combination of two revolute (2R) joints and three links which can be considered as a 2R planar manipulator. The augmented system is therefore an RP2R robot-needle mechanism.

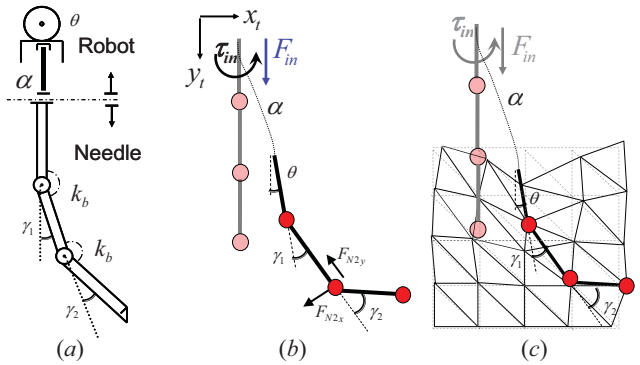

Fig. 1. Model of the needle as an RP2R planar manipulator with angular springs (a), external forces applied to the needle (b), and general model of a flexible needle inside a soft tissue modeled by finite element method (c).

Using the Newton-Euler formulation and the recursive algorithm described in [13], we have

$$\mathbf{M}(\mathbf{\Theta})\ddot{\mathbf{\Theta}} + \mathbf{C}(\mathbf{\Theta}, \dot{\mathbf{\Theta}}) = \mathbf{F}, \tag{1}$$

where, $\mathbf{\Theta} = [\alpha \ \theta \ \gamma_1 \ \gamma_2]^T$ is the vector of generalized coordinates, $\mathbf{M}$ is a 4×4 mass matrix, $\mathbf{C}$ is a 4×1 vector of Coriolis and centrifugal forces, and $\mathbf{F}$ is a 4×1 vector of augmented forces applied to the needle including the resistant forces due to the bending stiffness, input control force F_{in} and torque τ_{in} from the robot, and the interaction forces due to insertion. Interaction forces are drawn from three main sources: i) friction forces, ii) forces from the FEM of the tissue $\mathbf{F_w}$, and iii) asymmetric bevel-tip forces.

Friction forces are modeled by a combination of static and viscous friction components in a simplified Karnopp friction model [14] during the insertion phase (positive velocity)

$$F_f = (C_n + b_n\dot{\alpha})d \tag{2}$$

where C_n and b_n are model parameters and d is the insertion depth. Friction force is considered along the needle shaft and is applied to the needle at the nodes in contact with the tissue nodes that are previously cut by the needle. The interaction forces from the FEM of the tissue, which will be discussed in Section III, are applied perpendicular to the needle shaft for those links of the needle which are in contact with the cut nodes of the tissue. The asymmetric bevel-tip forces are derived from macroscopic force model proposed in [5] and applied to the last node of the needle. These forces will be discussed in Section IV.

III. FEM of the Soft Tissue

The soft tissue is modeled by an FEM in stick and slip modes shown in Figure 1(c). We consider the effect of FEM forces as external forces acting perpendicular to and along the needle links at the three nodes, *i.e.* $\mathbf{F_{Ni}} = [F_{Ni_x} F_{Ni_y}]$, in the coordinates attached to each link of the needle, as shown in the Figure 1(b) for the second link [10].

To derive these forces, we consider the interaction nodes of the tissue with the needle as the *working* nodes and the rest of the tissue nodes as the *non-working* nodes. If we

denote the forces and displacements of the working and non-working nodes as $\mathbf{F_w}$, $\mathbf{F_{nw}}$, $\mathbf{u_w}$, and $\mathbf{u_{nw}}$, respectively, and consider the tissue as an elastic object, then the forces at each node, are directly related to the movement of each FEM node according to [15]

$$\begin{pmatrix}\mathbf{F_w}\\ \mathbf{F_{nw}}\end{pmatrix} = \begin{pmatrix}\mathbf{K_{w1}} & \mathbf{K_{w2}}\\ \mathbf{K_{nw1}} & \mathbf{K_{nw2}}\end{pmatrix}\begin{pmatrix}\mathbf{u_w}\\ \mathbf{u_{nw}}\end{pmatrix} + \begin{pmatrix}\mathbf{C_{w1}} & \mathbf{C_{w2}}\\ \mathbf{C_{nw1}} & \mathbf{C_{nw2}}\end{pmatrix}\begin{pmatrix}\dot{\mathbf{u}}_\mathbf{w}\\ \dot{\mathbf{u}}_\mathbf{nw}\end{pmatrix} + \begin{pmatrix}\mathbf{M_{w1}} & \mathbf{M_{w2}}\\ \mathbf{M_{nw1}} & \mathbf{M_{nw2}}\end{pmatrix}\begin{pmatrix}\ddot{\mathbf{u}}_\mathbf{w}\\ \ddot{\mathbf{u}}_\mathbf{nw}\end{pmatrix} \quad (3)$$

where the block matrices $\mathbf{K_{w1}}, \mathbf{K_{w2}}, \mathbf{K_{nw1}}$ and $\mathbf{K_{nw2}}$ denote the tissue stiffness, $\mathbf{C_{w1}}, \mathbf{C_{w2}}, \mathbf{C_{nw1}}$ and $\mathbf{C_{nw2}}$ denote the tissue damping, and $\mathbf{M_{w1}}, \mathbf{M_{w2}}, \mathbf{M_{nw1}}$ and $\mathbf{M_{nw2}}$ denote the tissue mass matrices. If the nodes of the tissue and joints of the needle match, we have $\mathbf{F_{w}}_{6\times 1} = [F_{N1x}\ F_{N1y} \dots\ F_{N3x}\ F_{N3y}]^T$, otherwise F_{Nix} and F_{Niy} can be written as functions of the $\mathbf{F_w}$ components. The constrained tissue node displacements $\mathbf{u_w}$, caused by needle movement, and the derivatives of the displacements are applied at each iteration to the tissue and the forces of interaction $\mathbf{F_w}$ are numerically calculated from (3). These forces contribute to an augmented force vector $\mathbf{F}$, which is used through (1) to find $\mathbf{\Theta}$ and hence $\mathbf{u_w}$ for use in the next iteration. For the slip mode, in which the tissue is being cut, FEM forces along needle link directions are set to zero and only the friction forces are applied. The net amount of force at each node can be decomposed into parallel and perpendicular components in order to determine an effective stiffness at each node.

IV. Bevel-tip model and asymmetric forces

Asymmetric forces are applied to the needle-tip due to the bevel-tip asymmetry. These forces result in the needle bending during insertion and should be accounted in the mechanics-based dynamic model. Since we plan to develop a needle model, which relates the tissue forces to the amount of needle deflection based on the fundamental principles of mechanics, we require a model for the bevel-tip that fits this model, *i.e.* a model which gives the asymmetric forces applied to the last node of the flexible needle model developed in II-A. To the best of our knowledge, the only mechanics-based model for the bevel-tip forces has been proposed in [5], and we will use this model in ours to account for the asymmetric forces at the tip.

The resulting bevel-tip forces along and perpendicular to the needle shaft, defined as P and Q, are calculated by integrating the force distribution along the tip edges, which are assumed to be triangular in nature according to the observations made from macroscopic level experiments [5]. These forces are modeled as

$$P = \frac{K_T b^2}{2}\sin\lambda\left(\frac{\tan\lambda - \tan\beta}{1+\tan\lambda\tan\beta}\right) \quad (4)$$

$$Q = \frac{K_T b^2}{2}\cos\lambda\left(\frac{\tan\lambda - \tan\beta}{1+\tan\lambda\tan\beta}\right) - \frac{K_T a^2}{2}\tan\beta, \quad (5)$$

where K_T is a material property of the elastic phantom sensed by the needle which depends on both the physics of phantom and also the needle type, a and b are the lengths of bevel edges and λ is the bevel angle, as shown in Figure 2 [5]. We apply P and Q forces at the final node of the needle (needle tip) to simulate the bevel-tip needle. These forces contribute in the augmented force vector $\mathbf{F}$ in (1) through the Newton-Euler formulations. The driving force of the needle, generated from the base insertion force applied by the robot, acts at a point known as the *acting point* which is not necessarily at the centre of the needle [5]. The acting point, that depends on the needle type and tissue material, determines β and γ, as illustrated in Figure 2. The values reported for K_T are between $\sim 4\,kNm^{-2}$ and $\sim 13\,kNm^{-2}$ and the fraction $\frac{\beta}{\lambda}$ is reported between ~ 0.03 and 0.3 for different types of gels in [5].

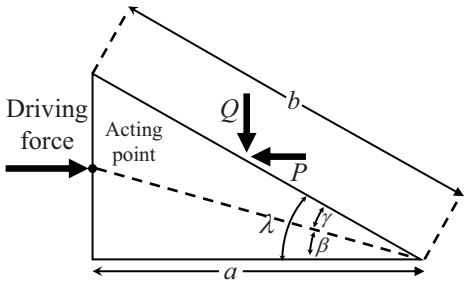

Fig. 2. Asymmetric forces acting on the needle tip [5]. The driving force of the needle does not necessarily act at the centre of the needle.

V. Experimental and Simulation Results

A. Experimental setup

The needle insertion experiments are performed on an experimental setup as shown in Figure 3. The testbed consists of a Quanser planar Twin Pantograph robotic manipulator equipped with a an ATI Nano-25 force/torque sensor connected through a needle holder to an 18 gauge $26\,cm$ brachytherapy needle with a 30° bevel angle. A Pointgrey Grosshopper (GRAS-20M4M-C) CCD camera, able to grab images with a maximum of $15\,Hz$, is mounted at the distance of $32\,cm$ above the PVC phantom fitted with a FUJINON 1:1.2/6mm DF6HA-1B optical lens. The stiffness of the PVC phantom could be adjusted by changing the portion of plastic and softener (or hardener). The PVC phantom used for this experiment was made of 5 portions of plastic and 1 portion of the softener[1]. For more information on the relation between the stiffness of the PVC and the portions of the plastic and the softener or hardener, the reader is referred to [16].

B. Simulation parameters

In order to simulate the combined model, we require different parameters including Young's modulus and Poisson's ratio for the FEM of the tissue, and K_T and the fraction β/λ for the bevel-tip model. The Young's modulus is estimated to be $\sim (76 \pm 6.0)\,kPa$ based on the values reported in [16] for the portion of plastic and softener used to fabricate the

[1]Supplier: M-F Manufacturing Co., Inc. Fort Worth, TX.

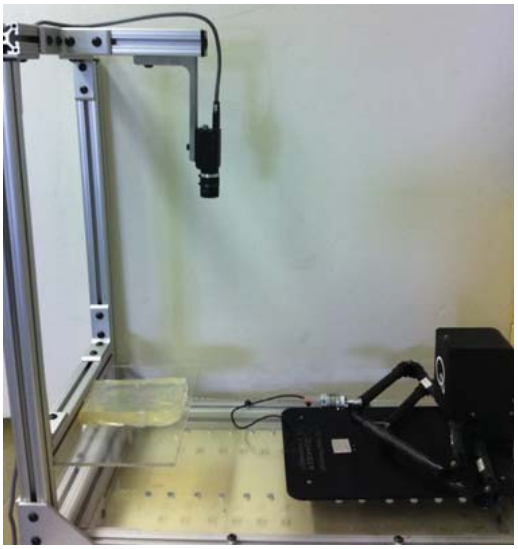

Fig. 3. Experimental setup consisting of a Twin Pantograph robotic manipulator equipped with a Nano-25 force/torque sensor, a CCD camera, a needle, and a PVC phantom.

TABLE I

TIP DEFLECTIONS FOR DIFFERENT FORCES APPLIED PERPENDICULAR TO THE NEEDLE SHAFT DURING IDENTIFICATION EXPERIMENTS.

Force (mN)	40	60	80	100	120	140	160
Deflection (mm)	21	28	33	37	47	51	55
γ_1	5°	7°	8°	9°	12°	13°	14°
γ_1	4°	5°	6°	6.5°	7.5°	8°	9°

phantom. It is also known that the Poisson's ratio for tissue-mimicking materials are less than 0.5. In this respect, we choose $\nu = 0.34$ for our simulations, based on the values reported in [17]. For the parameter K_T and the fraction β/λ, we tried different values in the range of values reported in [5] and compared the results with the experiments. The final choice of the parameters were $K_T = 9.42 \times 10^3$ and $\beta/\lambda = 0.2$, which have been used in the reported simulation results. The values used for parameters of the friction model 2 are empirically derived for the best fit which are $C_n = 6\,Nm$ and $b_n = 120\,N/m^2$. These values are within the same order of the values reported for a bovine liver in [14]. The bending stiffness parameter of the needle, *i.e.* k_b, was estimated as described next.

C. Needle angular-spring model parameter identification

The stiffness factor of the needle k_b was estimated by applying least squares to the data collected form the needle under static loads. Static forces within the range of $F_n = 40-160\,mN$ was applied at the needle-tip and perpendicular to the needle shaft, while images were taken from the bent needle. The images were visually matched with the three-link manipulator and and the two angles of the manipulator, i.e. γ_1 and γ_2, were determined. Table I shows needle deflections and determined joint angles for various tip forces.

The relation between the applied forces at the needle-tip and the manipulator joint angles is through the static

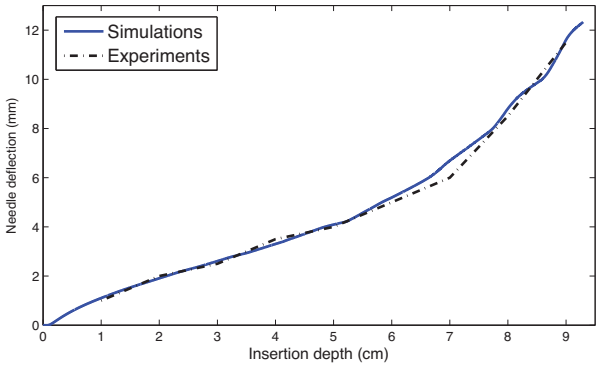

Fig. 4. Simulation and experimental results for needle deflections in different insertion depths.

relation $\tau = \mathbf{J}^T\mathbf{F}$, where $\mathbf{J}$ is the manipulator Jacobian and τ is the vector of torques induced at the joints, which are linearly related to the joint angles. The above relation can be expanded as

$$\begin{pmatrix} k_{b1} & 0 \\ 0 & k_{b2} \end{pmatrix}\begin{pmatrix} \gamma_1 \\ \gamma_2 \end{pmatrix} = \begin{pmatrix} -L_1 s_1 - L_2 s_{12} & L_1 c_1 + L_2 c_{12} \\ -L_2 s_{12} & L_2 c_{12} \end{pmatrix}\begin{pmatrix} 0 \\ F_n \end{pmatrix} \quad (6)$$

where k_{b1} and k_{b2} are bending stiffness factors at the joints, L_1 and L_2 are the link lengths, and s_i, c_i, s_{ij}, and c_{ij} represent $\sin(\gamma_i)$ and $\cos(\gamma_i)$, $\sin(\gamma_i+\gamma_j)$, and $\cos(\gamma_i+\gamma_j)$, respectively. Assuming uniformity across the needle, that is $k_{b1} = k_{b2}$, without loss of generality, we can rewrite (6) as

$$k_b\mathbf{\Phi} = \mathbf{Y}, \quad (7)$$

where $\mathbf{\Phi} = [\tilde{\gamma}_1 \;\; , \;\; \tilde{\gamma}_2]$ and $\mathbf{Y} = [(L_1c_1 + L_2c_{12})\tilde{F}_n \;\; , \;\; L_2c_{12}\tilde{F}_n]$ are matrices denoting an ensemble of measured quantities for multiple sampling points. Using the Least-Squares, the parameter k_b can be estimated from

$$k_b = (\mathbf{\Phi}^T\mathbf{\Phi})^{-1}\mathbf{\Phi}^T\mathbf{Y}. \quad (8)$$

Substituting the values reported in Table I in $\mathbf{\Phi}$ and $\mathbf{Y}$ and using (8), considering $L_1 = L_2 = 26/3\,cm \approx 87\,mm$, the needle stiffness $k_b \approx 0.092\,Nm$ is achieved with the mean-square-error (MSE) of $5.3e^{-6}$. For high number of nodes (joints), a more efficient method has been presented in [11].

D. Experiment and simulation results

The experiment consists of inserting needle in the radial (along the y axis) direction at the nominal speed of $\sim 6\,mm/sec$. The goal is to compare the traversed path and needle deflections obtained from the experiment and simulation for various depths. The insertion angle θ and depth α are controlled in both simulations and experiments using the control signals F_{in} and τ_{in}. The insertion angle set-point is zero degree.

Figure 4 shows the results of deflections versus the insertion depth for both simulation and experiments. The maximum error between simulation and experiment is $0.5\,mm$ at the depth of $7\,cm$. It is important to note that the accuracy

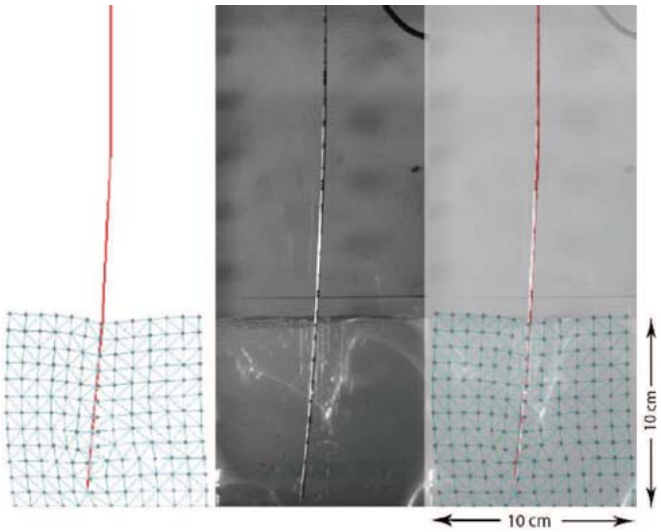

Fig. 5. Simulation and experimental result for the final instant of insertion, when the insertion depth is $9\,cm$. From left to right: simulation, experiment, and the superimposed images.

of the measured deflections from the collected images is $0.5\,mm$.

Figure 5 shows snap shots of the needle in both the experiment and simulation and their superimposed image at the final instant of insertion when the insertion depth is $9\,cm$. It is observed that the model can mimic the actual needle pose visually accurately. The single degree-of-freedom (DOF) experiment and simulation have been performed to evaluate the model in single direction similar to experiments conducted in [8]. The model can be evaluated in two DOFs by rotating the needle base during insertion through application of different torques to the base which will be considered as a future work.

VI. Conclusions

In this paper we have developed a complete mechanics-based dynamic model for bevel-tip flexible needles and have reported preliminary results from the validation experiments. The model is unique in the sense that it predicts needle deflections and tissue deformations at the same time, determines the insertion progression over time, and is suitable for dynamic feedback control of needle insertion. The model excited in radial direction predicts actual needle deflection with the maximum sensory accuracy, *i.e.* $\sim 0.5\,mm$. Future works will aim towards the evaluation of the model for various insertion speeds, variable insertion angle and controllability analysis of needle-tissue model for feedback control design.

VII. Acknowledgments

This work was supported in part by Natural Sciences and Engineering Research Council of Canada (NSERC) and Queen's University Advisory Research Committee (ARC).

References

[1] G. Fichtinger, T. DeWeese, and A. Patriciu et. al., "System for robotically assisted prostate biopsy and therapy with intraoperative CT guidance," *Acad Radiol*, vol. 9, no. 1, pp. 60–74, 2002.

[2] R. Alterovitz, J. Pouliot, R. Taschereau, I. Hsu, and K. Goldberg, "Simulating needle insertion and radioactive seed implantation for prostate brachytherapy," *Stud. in Health Tech. and Informat.*, pp. 19–25, 2003.

[3] N. Abolhassani, R. Patel, and M. Moallem, "Needle insertion into soft tissue: A survey," *Med. Eng. and Phys.*, vol. 29, no. 4, pp. 413–431, 2007.

[4] R. Webster, J. Kim, N. Cowan, G. Chirikjian, and A. Okamura, "Nonholonomic modeling of needle steering," *The Intl. J. of Rob. Res.*, vol. 25, no. 5-6, p. 509, 2006.

[5] S. Misra, K. Reed, B. Schafer, K. Ramesh, and A. Okamura, "Mechanics of flexible needles robotically steered through soft tissue," *The Intl. J. of Rob. Res.*, vol. 29, no. 13, p. 1640, 2010.

[6] K. Reed, A. Okamura, and N. Cowan, "Modeling and control of needles with torsional friction," *IEEE Trans. on Biomed. Eng.*, vol. 56, no. 12, pp. 2905–2916, 2009.

[7] H. Kataoka, T. Washio, M. Audette, and K. Mizuhara, "A model for relations between needle deflection, force, and thickness on needle penetration," in *Proc. of Med. Im. Comp. and Comp.-Assis. Inter.*, 2001, pp. 966–974.

[8] N. Abolhassani and R. Patel, "Deflection of a flexible needle during insertion into soft tissue," in *Proc. of Intl. Conf. of the IEEE Eng. in Med. and Bio. Soc.*, 2006, pp. 3858–3861.

[9] K. Hauser, R. Alterovitz, N. Chentanez, A. Okamura, and K. Goldberg, "Feedback control for steering needles through 3D deformable tissue using helical paths," *Rob. Sci. and Sys.*, 2009.

[10] A. Haddadi, O. Goksel, S. Salcudean, and K. Hashtrudi-Zaad, "On the controllability of dynamic model-based needle insertion in soft tissue," in *Proc. of Intl. Conf. of the IEEE Eng. in Med. and Biol. Soc.*, 2010, pp. 2287–2291.

[11] O. Goksel, E. Dehghan, and S. E. Salcudean, "Modeling and simulation of flexible needles," *Med. Eng. and Phys.*, pp. 1069–1078, 2009.

[12] S. Misra, K. Reed, K. Ramesh, and A. Okamura, "Observations of needle-tissue interactions," in *Proc. of Intl. Conf. of the IEEE Eng. in Med. and Biol. Soc.*, 2009, pp. 262–265.

[13] L. Sciavicco, B. Siciliano, and B. Sciavicco, *Modelling and Control of Robot Manipulators*, 2nd ed. Secaucus, NJ, USA: Springer-Verlag New York, Inc., 2000.

[14] A. Okamura, C. Simone, and M. O'Leary, "Force modeling for needle insertion into soft tissue," *IEEE Trans. on Biomed. Eng.*, vol. 51, no. 10, pp. 1707–1716, 2004.

[15] S. P. DiMaio and S. E. Salcudean, "Interactive simulation of needle insertion models," *IEEE Trans. on Biomed. Eng.*, vol. 52, no. 7, pp. 1167–1179, 2005.

[16] A. Baghani, H. Eskandari, S. Salcudean, and R. Rohling, "Measurement of viscoelastic properties of tissue-mimicking material using longitudinal wave excitation," *IEEE Trans. on Ultr., Ferroelec. and Freq. Cont.*, vol. 56, no. 7, pp. 1405–1418, 2009.

[17] S. P. DiMaio and S. E. Salcudean, "Needle insertion modeling and simulation," *IEEE Trans. on Rob. and Auto.*, vol. 19, no. 5, pp. 864–875, 2003.